John B. Goodenough: Tribute to John B. Goodenough: From Magnetism to Rechargeable Batteries (Adv. Energy Mater. 2/2021)

Alain Mauger, Christian Julien, Michel Armand, Karim Zaghib

Tribute to John Goodenough: from magnetism to rechargeable batteries

A. Mauger[1], C. Julien[1], M. Armand[2], and K. Zaghib[3]*

1Institut de Minéralogie, de Physique des Matériaux et de Cosmochimie (IMPMC), Sorbonne Université, UMR-CNRS 7590, 75005 Paris, France
2CNRS UMR-6007, Université de Picardie Jules Verne, Amiens, France.
3Centre of Excellence in Transportation Electrification and Energy Storage (CETEES), Hydro-Québec, 1806, Varennes, QC J3X1S1, Canada

Corresponding author: zaghib.karim@hydro.qc.ca

Abstract

In macroeconomics, the rate of economic growth in the world is a historical phenomenon which will mark the 20th century. It was made possible by an increasing consumption of fossil fuel. However, not only these resources are limited and not renewable, but also there combustion have dramatic side effects such as emission of greenhouse gases responsible for a global warming and change of climate. As a consequence, major efforts are taken to move away from fossil fuels and switch to renewable energy including solar and wind energy. These energy sources, however, are intermittent and can be integrated into the electrical network only after regulation. The electrochemical storage is a key solution to regulate these intermittent sources of energy into smart grids. Although the politicies that govern have only recently become aware of this problem, some scientists focussed their attention on rechargeable batteries since the 70s, and it took until 2019 to the Nobel committee to award the Nobel price to those who paved the path to their development. John Goodenough is one of the three winners of this Nobel price, for his pioneering research on lithium-ion batteries (LIBs). The impact of LIBs includes the development of rechargeable hybrid and electric vehicles at the expense of gasoline cars. Before the 70s, however, John Goodenough had already made major contributions to materials science as a solid state physicist, including the investigation of the interplay between the magnetic and transport properties of perovskites. It is the purpose of the present work to report a brief review of the scientific works of John Goodenough, through selected works that herald the wedding between chemistry and physics.

Key Word; John B Goodenough, magnetism, LiCoO2, lithium, rechargeable batteries

I. Introduction

In 2019, Professor John B. Goodenough was awarded the Nobel Prize in Chemistry, as a recognition for his pioneering works and contribution to the development of Li-ion batteries. The

media input of this price might hide the outstanding contribution of Goodenough in solid-state physics. Indeed, as a first step John is a solid-state physicist, which guided him to work on different problems including transition-metal transitions [1,3], high-Tc superconductivity [4-11], phase segregation [12]. Citation bases indicate that 643 out of the 1092 publications he co-signed belong to physics. It is then impossible to make an exhaustive report on his contributions not only in chemistry, but also in physics. We have chosen to select magnetism as one topic in physics. One reason is that we are indebted to John for the investigation of the superexchange interactions in transition-metal compounds leading to the so-called Goodenough-Kanamori rule that is one of the most important rules in ligand field theory. The other reason is that these rules are very useful to characterize materials used as electrodes in rechargeable batteries, so that it makes contact between contributions of Goodenough in physics and chemistry. As expected, the second part of this review is devoted to an illustration of the contributions of John Goodenough to the research and development of rechargeable batteries.

II. Magnetic properties of transition metal oxides

The Goodenough-Kanamori (GK) rule gives the sign (ferromagnetic or antiferromagnetic) of the magnetic interactions in semiconducting or insulating compounds. In metals, the dominating exchange interactions are indirect exchange mediated via the conducting electrons and are thus of a different nature. However, all the active materials for electrodes of rechargeable batteries are either insulating or at best semiconducting. In this case, the orbital momentum of the transition ions is quenched by the crystal field, and the magnetic interactions between the transition ions are dominated by the spin-spin superexchange interactions so that the GK rule applies. This rule has been formulated first by Goodenough in 1955 [13,14] and a rigorous mathematical demonstration was provided by Kanamori [15,16]. An exhaustive report on the sign of the magnetic interactions for the different occupations of the *d*-states of the transition ions and the different geometric configurations is now of practical use to know the sign and the relative strength of the magnetic interactions in any non-metallic transition compounds [17]. The rule states that superexchange interactions (SIs) are antiferromagnetic, where the virtual electron transfer is between overlapping orbitals that are each half-filled. SIs are ferromagnetic where the virtual electron transfer is from a half-filled to an empty orbital or from a filled to a half-filled orbital. Note the SIs mediated by virtual electron transfers between the magnetic ions are not the only ones. There are also magnetic interactions between a shared anion and the two magnetic ions, called semi-covalent interactions, but the GK rule also applies to them.

John Goodenough applied the rule to understand the magnetic properties of perovskites. As we

shall see later in this review, perovskites have applications in rechargeable batteries, but they are very attractive for many other device applications, particularly in photovoltaic cells. Their crystal structure is illustrated in Fig. 1. The first example was $LaFeO_3$, in which Fe has a valency of 3+ in the configuration t^3e^2 corresponding to the d^5 high-spin ground state [17]. Under the effect of the cubic crystal field, the five-orbital *d*-states are split in three *t*-orbital states (ground states) and two *e*-orbital states. Therefore, in $LaFeO_3$ all the *d*-states are half-filled. According to the GK rule, each of them give antiferromagnetic interactions, so that the Fe–O–Fe interactions are antiferromagnetic. Actually, a cooperative Jahn-Teller effect induces a small lattice distortion that induces a transition from cubic to orthorhombic phase (space group *Pbnm*) as illustrated in Fig. 1, but in such a particular material, this distortion is much too small to have a significant effect on the magnetic interactions. Another example is $LaCrO_3$ [18]. The Cr^{3+} ions in the octahedral sites are in the t^3e^0 state. As in the previous case the three *t*-electrons give antiferromagnetic π-bond superexchange interactions. The two *e*-orbitals cannot generate superexchange interactions since they are empty, but they generate antiferromagnetic σ-bond spin-spin interactions via a semicovalent-exchange interaction. Therefore, the material in the orthorhombic (O) phase exhibits the G-type antiferromagnetic spin order at ambient pressure. The G type stands for an isotropic antiferromagnetic coupling of a given Cr^{3+} with the six magnetic neighbors. A first order transition to the rhombohedral (R) phase can be obtained by application of pressure, allowing Zhou et al. used to explore how the magnetic phase enters the R-phase under high pressure (see Fig. 2). The antiferromagnetic nature of t^3-oxygen-t^3 determined by the GK rule is not modified at the transition and the material remains antiferromagnetic. However, the spin-ordering direction is degenerate in the O-phase, while the *R*-3*c* group symmetry only allows the antiferromagnetic spin structure with the spin direction along the *c* axis. Therefore, the spin direction rotates from pointing to the octahedral edge in the O-phase to perpendicular to the triangle plane of the octahedra in the R-phase (Fig. 1). This illustrates the interplay between the magnetic properties and the structure in the perovskites, and this study has revealed a general rule for spin direction in antiferromagnetic perovskites RMO_3, where *R* is a rare earth ion and *M* a transition ion, both in the trivalent state [19]:(1) it is parallel to the rotation axis with the highest symmetry in the space group; (2) if there are more than one rotation axis in the space group, it is determined by either higher-order orbital angular momentum or the *R*-*M* exchange interaction for the magnetic rare earth. Another perovskite of interest is $LaMnO_3$ [20]. Mn^{3+} is in the high spin configuration t^3e^1. In this configuration, a gain in energy results by a lattice distortion that lifts the two-fold degeneracy of the e-orbital states, so that Mn^{3+} is a Jahn-Teller ion. As a result of this cooperative Jahn-Teller distortion, long and short O–M–O bonds alternate along

the cubic [100] and [010] axes, ordering half-filled σ-bond orbitals of e parentage in the long O–Mn–O bonds and empty σ-bond orbitals in the short O–Mn–O bonds of the (001) planes. Due to the orbital ordering, half-filled σ-bond orbitals overlap empty σ-bond orbitals in the (001) planes to give ferromagnetic interactions, whereas the half-filled π-bonding t orbitals give t^3-oxygen-t^3 antiferromagnetic interactions between all near neighbor Mn^{3+} ions. However, since the overlap of the σ-bond electrons is larger than that of the π-bond electrons, the ferromagnetic interactions are stronger in the (001) plane, and the t^3-oxygen-t^3 couple antiferromagnetically the ferromagnetic (001) planes. This study has been completed by substituting R^{3+} rare-earth ions for the La^{3+} ion [21]. The strength of the σ-bond ferromagnetic interaction decreases relative to the antiferromagnetic π-bond interactions with increasing atomic weight of the R^{3+} ion until the π-bond and σ-bond interactions within the (001) planes become of comparable magnitude, at which point an exchange-density wave appears. The ligand field theory can also be used to understand why $LaCoO_3$ is ferromagnetic [22]. These studies are just examples among a huge number of studies published on the perovskites with the *Pbnm* space group and its subgroup *P*21/*m* since the space groups accommodate all antiferromagnetic and ferromagnetic spin-ordering phases [23]. In case the orbital momentum is not quenched, perovskites have remarkable and complex magnetic properties, and we are indebted to Goodenough for their understanding [24]. The concept of cooperative orbital ordering in transition-metal compounds investigated in this context proved key to realization of the first random-access memory (RAM) [25]. Closer to the energy storage context, Goodenough et al. identified design principle for oxygen-reduction activity on perovskite oxide catalysts for fuel cells and metal-air batteries, demonstrating that the oxygen reduction reaction (ORR) activity for oxide catalysts primarily correlates to σ-e_g occupation and the extent of *B*-site transition-metal covalency, which serves as a secondary activity descriptor [26].

Among materials crystallizing in other structures, spinels of general formula AB_2O_4 containing transition metal ions are among the most studied materials in solid-state science, due to their wide range of applications, as photocatalysts and catalysts in various chemical reactions, including carbon monoxide (CO) oxidation, catalytic combustion of hydrocarbons, reduction of several organic molecules (see [27] and references therein), and some of them are also active elements for positive electrodes (see below). Depending on the valence states X^{2+}, Y^{3+}, Z^{4+} of the *A* and *B* ions, the cation distribution is given by the chemical formulas $Z(X_2)O_4$, $X(ZX)O_4$, $X(Y_2)O_4$ or $Y(XY)O_4$, where the ions within the parentheses occupy octahedral sites, while the ions in front of the parentheses occupy tetrahedral sites. The physical properties depend importantly not only on the nature of the cations, but also on their distribution on the octahedral and tetrahedral sites. It is actually in an attempt to

understand this distribution that Goodenough and Loeb introduced the concept of semicovalent exchange above- mentioned [28]. In this work, they showed that it is possible to predict nearly all the observed cation distributions and the magnetic properties of the spinels from only qualitative considerations taking the covalent and semicovalent interactions into account. To understand the powerful tool that Goodenough found with such concepts in the context of spinels, we report two examples. Let us first consider $ZnCr_2O_4$, where the Cr^{3+}: t^3e^0 ions occupy octahedral sites, so that only 90° Cr – anion – Cr magnetic interactions are associated with a shared anion. After the Goodenough-Kanamori rules, there are two competing interactions: the antiferromagnetic t^3-t^3 superexchange interactions across a shared octahedral-site edge and the ferromagnetic 90° Cr^{3+} – anion – Cr^{3+} interactions. Since the Cr–Cr separation is short and the covalent component is weak, the antiferromagnetic interaction is dominant and the material is antiferromagnetic. Such spinels are now under studies not only for their applications, but also because they are archetypes of frustrated systems, and the effect of frustration is a domain of research *per se* in magnetism.

The positive cathode active elements of rechargeable batteries are transition-metal compounds. In addition, any electrochemical process involves a change in the valence of the transition ions. Therefore, the study of the magnetic properties of these cathode elements is a tool, not only to characterize them, but also to analyze the reactions involved in the electrochemical processes. We have reported elsewhere such investigations for many cathode elements [29], and only recall here that we are largely indebted to Goodenough who gave the bases allowing such investigations.

III. Rechargeable batteries

A. Li-ion batteries with liquid electrolytes

John Goodenough has been awarded the Nobel Prize for his pioneering works in lithium-ion batteries (LIBs), as recalled in the history of their early developments [30]. Identified and tested by Goodenough, $LiCoO_2$ is the cathode that was used in the first commercialized LIB [31,32]. Three decades later, it is still widely used. $LiCoO_2$ is the archetype of cathode materials with two-dimensional structure (lamellar compounds). They consist of transition-metal ions in edge-shared interstices between pairs of close-packed anion planes; these planes bond to one another by van der Waals forces between anion planes. The mobile Li^+ ions are inserted into the van der Waals gap, so that the motion of the lithium is two-dimensional (2D). The success of $LiCoO_2$ was the motivation for the investigation of many other 2D-cathode materials; they have been reviewed in Chapter 5 of Ref. [29].

Since the 2D framework, the nature of motion might reduce the mobility of Li^+ ions, Goodenough and Thackeray explored the implications of an earlier report [33] that Li^+ ions can be inserted into the spinel Fe_3O_4, which has an interstitial space with 3D interconnections [34], and they proposed $LiMn_2O_4$ because it offers the possibility of having only Li^+ ions in the interstitial space of the $[Mn_2]O_4$ framework [35]. Indeed, the material $Li_xMn_2O_4$ can be cycled in the 4-volt region in the range $0 \leq x \leq 1$, i.e. between λ-MnO_2 and $LiMn_2O_4$. It can also be cycled in the range $1 \leq x \leq 2$ but a cubic-tetragonal crystallographic phase transition change does not allow to maintain the structural stability of the cathode, so that in practice, the battery can be cycled only in the range $0 \leq x \leq 1$ with a specific capacity of 120 mAh g^{-1} comparable to the theoretical capacity of 140 mAh g^{-1}. Still in this 4-volt domain, $LiMn_2O_4$ tends to show a capacity fading due to dissolution of the manganese in the liquid electrolyte, especially at elevated temperature. Nevertheless, the battery manufacturers still use $LiMn_2O_4$ as a cathode material, but they add another active element that traps manganese. This additive element is a lamellar compound: $LiNiAlO_2$ for AESC that equipped the LIBs for Nissan (Japan) electric cars until 2018, or $Li(NiMnCo)O_2$ (NMC) by LG Co. (Korea). Spinels can also find applications in Li-air batteries. For instance, $CoMn_2O_4$ spinel nanoparticles grown on graphene can provide a catalytic platform of considerable activity for cycling Li-air cells [36]. Investigation of the high-voltage $Li[Ni_{0.5-x}Mn_{1.5+x}]O_4$ (x = 0, 0.05, 0.08) spinels shows that removal of the Ni^{4+}/Ni^{2+} redox reactions from the surface stabilizes the electrochemical performance at 55 °C, but the problem of Mn^{2+} dissolution resulting from surface disproportionation of Mn^{3+} to Mn^{2+} and Mn^{4+} still remains [37]. The spinel $LiNi_{0.5}Mn_{1.5}O_4$ and most of all its related Cr-doped structure are now considered are the archetypes of cathode materials of the 5-volt class [38]. The Cr doping increases both the kinetics of the Li^+-ion insertion/extraction and the structural stability [39] (see Fig. 3).

In 1997, John Goodenough proposed $LiFePO_4$ as an active material for the positive electrode of rechargeable Li-ion batteries [40]. The redox couple Fe^{3+}/Fe^{2+} at 3.5 V *vs.* Li^+/Li lies in the electrochemical window for stability of the liquid electrolytes [41]. In pure $LiFePO_4$, the iron ion is in the Fe^{2+} valence state. Fe^{2+} is a Jahn-Teller ion only if it is in a tetrahedral site [42], and in $LiFePO_4$ it is located in an octahedral site. The absence of Jahn-Teller lattice distortion and the strong covalent bonding of the PO_4 units insure a very good structural and thermal stability. There were, however, two difficulties to overcome. First, this material is a very poor electronic conductor, which was overcome by coating the particles with some conductive form of carbon. The electrodeposited carbon-coated $LiFePO_4$/polypyrrole (PPy/C-$LiFePO_4$) composite exhibits the best performance to enhance the capacity at high rates of charge and discharge by substitution of a conductive, electrochemically active

polymer for some or all of the deadweight conductive carbon and binder used conventionally [43,44]. PPy/C-$LiFePO_4$ composites required no additional carbon or binder and gave a superior capacity at high rates. The success of this strategy has two origins: (i) the electrodeposition ensures a good electrical contact between particles and current collector as well as between particles, and (ii) the electroactive range of the polymer overlaps the operative redox couple (3.5 V). An excellent charge/discharge performance at a rate as high as 10C, and even a 3 min (20C) charge, is demonstrated with a C-$LiFePO_4$/PPy cathode containing 16 wt % PPy [45]. This is just an illustration of the fact that the route to new applications, from hybrid electric vehicles to high-power electronics and regulation of the intermittency problem of electric energy supply on smart grids, has been opened by the surface modification and the synthesis of new multi-composite particles of active materials for positive electrodes [46]. Second, the diffusion of Li^+ ions in $LiFePO_4$ is a one-dimensional motion, implying that the electrochemical performance is very sensitive to impurities, since any impurity can block not only one Li^+ ion, but all the ions in a channel. As a matter of fact, iron prefers to be in a trivalent state in nature, and the presence of impurities that contain Fe^{3+} ions in (uncoated) $LiFePO_4$ is inevitable. Fortunately, the coating process reduces the Fe^{3+}-impurities that poison $LiFePO_4$, an essential step to obtain a material with good electrochemical properties [47]. The reason is not due to the carbon itself, but to the fact that the carbon precursor is (and must be) an organic material that also contains hydrogen. The hydrogenic species formed by the decomposition of the precursor during the coating process reduce Fe^{3+}, thus allowing the synthesis of pure carbon-coated $LiFePO_4$ [48]. In $LiFePO_4$, the intra-atomic Fe^{2+}-Fe^{3+} transitions suffer a strong Franck-Condon effect due to the local distortion of the lattice in $FePO_4$, which is indirect evidence of the formation of a small polaron. The nearest iron neighbors around the central polaron site are spin-polarized by the indirect exchange mediated by the electronic charge in excess. These small polarons are thus magnetic, and responsible for the interplay between electronic and magnetic properties that were self-consistently and quantitatively determined [49] (see Fig. 4). The analysis of magnetic properties was not only useful to understand the polaron-type of electronic conductivity associated with the presence of Fe^{3+} due to Li^+ vacancies. It also allowed to identify the impurities and quantify their concentration [50]. On the one hand, iron is a magnetic ion and the impurities can be identified by their Neel or Curie temperature detected by magnetic measurements. On another hand, the analysis of the magnetic measurements is a much more sensitive tool than X-ray diffraction analysis to quantify the amount of such impurities. The strategy used to optimize the electrochemical properties has thus been to determine which impurities poison this material by the analysis of the magnetic properties, and modify the synthesis parameters to get rid of

them, until pure samples could be obtained [50]. These investigations also led to an overall understanding of all the structural, physical and electrochemical properties of this material, which conquered an important part of the market of LIBs, in particular in Asia [51].

For some applications, in particular electric vehicles (EVs), there is a need to increase the energy density to improve to increase the driving range. One way to do it is to increase the redox voltage. Within the family of olivines, this led to consider the replacement of Fe by Co or Ni, which would raise the working potential to 4.8 and 5.1 V *vs*. Li^+/Li, respectively. The potential of 5.1 V provided by $LiNiPO_4$ is too high to avoid oxidation of the liquid electrolytes that are currently used, and the antisite problem due to the fact that the ionic radii of Li^+ and Ni^{2+} are almost the same, is another problem. There is thus little hope that this material can find applications. On another hand, $LiCoPO_4$ is more promising, as it is now possible to achieve a stable capacity of 140 mAh g^{-1} over 250 cycles [52].

In practice, all the commercial LIBs, except the Bluecar of Bolloré, use carbonate-based liquid electrolytes, because they have a high-ionic conductivity. The improvement of the lithium batteries with such electrolytes has been obtained by decreasing the size of the active particles of the electrodes to few tens of nanometers, but also by surface modification and the synthesis of new multi-composite particles [46]. However, such electrolytes are not compatible with Li-metal and their use result in the formation of dendrites at the surface of the lithium metal, which is damageable for the cycling life and safety issues. That is why the anode of the commercial batteries is made of graphitic carbon. However, many efforts of research are currently done to replace the graphitic carbon by a lithium metal anode, as it would increase importantly the energy density. One solution to avoid the contact between metallic-lithium anode and an organic-liquid electrolyte is to use a low-cost cellulose-based porous membrane separator that acts as the solid electrolyte interphase (SEI) at the anode–electrolyte interface. Cells with this membrane as separator show excellent, safe electrochemical performance of Li-anode cells and organic-liquid electrolytes for up to 1000 cycles [53]. Lithium is very reactive and must be protected against humid air, which makes the fabrication of the batteries more expensive. A solution to reduce the price of the battery is to make a hydrophobic artificial SEI. As shown by the Goodenough group, a composite Li anode containing a protective layer consisting of lithium fluoride and graphite fluoride fills the purpose [54]. The corresponding anode exhibits a safe and dendrite-free cycling at a current density from 1 to 10 mA cm^{-2} for a long cycle life in the Li stripping/plating experiments. After exposure to a humid atmosphere with RH of 20–35% for over 24 h, it provides a comparable specific capacity and cycling stability as fresh Li-metal anodes that have not been exposed to air.

Some attempts have been made to use additives to the liquid electrolytes to make them compatible

with Li metal. So far, however, additives reduce the formation of dendrites, but fail to suppress them. It is presently believed that the most promising strategy to replace the graphitic carbon anode by lithium metal is to replace the liquid electrolyte by a solid electrolyte to avoid the formation of dendrites. In addition, it would increase the safety of the batteries, since the carbonates are flammable and are responsible for battery fires in case of misfunction. Many solid electrolytes, either ceramics or polymers, are only prepared and studied as very thick films (sometimes over 100 μm). However, using thick films dramatically diminish the cell-level energy density, preventing the implementation in a high-energy cell at a commercial level. Pathways to obtain homogeneous and thinner electrolyte films have been proposed [55]. Two kind of solid electrolytes are currently under investigations: polymers and solid-state ceramics. Both of them have been explored by Goodenough.

B. All solid-state lithium batteries

No single polymer has a large enough energy gap between the empty and occupied electronic states for both dendrite- free plating of a lithium- metal anode and a Li^+ extraction from an oxide host cathode without electrolyte oxidation in a high- voltage cell during the charge process. On another hand, a bilayer polymer electrolyte with a high- voltage stable layer contacting cathode and a low- voltage stable layer contacting anode is a strategy to obtain an electrolyte. Poly(*N*- methyl- malonic amide) (PMA) that contains a repeating unit of high dielectric constant dimethylacetamide on the cathode side [56], and a PEO–LiTFSI layer on the lithium metal anode fill the requirements and satisfy the purpose. The all-solid-state Li/PEO–LiTFSI/PMA–LiTFSI/$LiCoO_2$ cells tested at 65 °C delivered a capacity of 108.5 mAh g^{-1} at 0.2 C after 100 cycles, which corresponds to a retention of 91.2%. At a larger C rate of 1 C, a stable cycling performance was obtained with a charge/discharge capacity of 57 mAh g^{-1} [57]. Another difficulty in using polymers is to meet simultaneously requirements of a mechanical strength large enough to block the formation of dendrites, but with an ionic conductivity good enough to be used in a battery. Again, it is difficult to obtain simultaneously both requirements with a single polymer, the reason why cross-linking of two polymers is a good strategy. Nevertheless, the ionic conductivity of such polymeric electrolytes remains smaller that of ionic liquids. On another hand, some ceramics have a very high ionic conductivity and their interest as oxide-ion electrolytes for use in solid-state batteries has been recognized since decades [58]. However, it is difficult to use ceramic films as electrolytes, for different reasons. Some of them are difficult to prepare, and are sensitive to moisture. Eventually, they are not compatible with electrodes. On the cathode side for example, $Li_7La_3Zr_2O_{12}$ (LLZO), the structural and transport properties of which

have been investigated by the Goodenough group [59,60], is not compatible with $LiCoO_2$, and it is important to separate direct contacts between $LiCoO_2$ and pure LLZO by a surface modification of LLZO (e.g., Co-diffused surface layer and/or presence of an interlayer, Li_3BO_3) [61]. Usually, LLZO is doped to improve its conductivity. In particular, the garnet-related oxides with the general formula $Li_{7-x}La_3Zr_{2-x}Ta_xO_{12}$ have the highest Li^+ conductivity 1.0×10^{-3} S cm^{-1} for $x = 0.6$ with an activation energy of 0.35 eV in the temperature range of 298-430 K, which makes this Li-ion solid electrolyte attractive [62]. Such garnet-structured oxides are promising solid Li-ion electrolytes for all-solid-state Li-metal batteries, provided the Li_2CO_3 layer and the Li-Al-O glass phase surface of garnet materials are removed from the surface of the garnet materials by appropriate thermal treatment in presence of carbon [63] (see Fig. 5). Another improvement consists in the addition of LiF to increase the stability of the garnet electrolyte against moist air [56]. In this work, Li et al. fabricated an all-solid-state Li/polymer/$Li_{6.5}La_3Zr_{1.5}Ta_{0.5}O_{12}$ (LLZT)-2 wt.% LiF/$LiFePO_4$ battery with high Coulombic efficiency keeping 93% of its capacity after 100 cycles. The LLZT-2 wt.% LiF electrolyte separator blocked the polysulfide transport towards the Li-metal. Coating the garnet with a blend made of poly(ethylene oxide) (PEO) and lithium poly(acrylamide-2-methyl-1-propane-sulfonate) (PAS) was also shown to suppress dendrite formation and to reduce greatly the interfacial resistance, because the coordinating interaction of ethylene-oxide in PEO and lithium-ion pendants in PAS facilitates the movement of Li^+ along the PEO long chains. The capacity retention of the all-solid-state Li/coated-garnet/$LiFePO_4$ at 65 °C was 137 mAh g^{-1} at 0.2 C after 160 cycles [64].

Another difficulty met with ceramics come from the grain boundaries that create gradients of the electric potential, responsible for the growth of lithium dendrites. Moreover, the solid contact between the ceramic and the electrode is usually made by contact points rather than a uniform contact between the layers. And finally, since the volume of the electrolyte and the electrodes varies during cycling, it is very difficult to maintain the solid contact between them. Therefore, the polymer film between the lithium and the ceramic is also here to act as a buffer between the lithium layer and the ceramic film [55]. In the same way, a sandwich electrolyte of polymer/ceramic-pellet/polymer was successfully used to plate a dendrite-free lithium anode, where the polymer was the cross-linked poly(ethylene glycol) methyl ether acrylate (CPMEA) [65]. The cross-linked poly(ethylene glycol) methyl ether acrylate (CPMEA) established a three-dimensional network containing a polyacrylate main chain and oligoethylene oxide pendants terminated by $-OCH_3$ units, with LiTFSI as the salt. A ceramic membrane of NASICON-structured $Li_{1.3}Al_{0.3}Ti_{1.7}(PO_4)_3$ (LATP) was employed. The capacity retention of Li//$LiFePO_4$ cell using this PCPSE was still around 102 mAh g^{-1} at 0.6C (0.51 mA cm^{-2}) after 640

cycles. This result illustrates the success of this strategy. The introduction of the ceramic layer blocks anion transport, which reduces the double-layer electric field at the Li/polymer interface and lowers the chemical/electrochemical decomposition of the polymer electrolyte to improve the Coulombic efficiency of a battery. On the other hand, a polymer electrolyte layer that is between the anode and a ceramic electrolyte can suppress dendrite nucleation due to the uniform Li^+ flux on the polymer/lithium interface and better wetting ability toward lithium metal and protects the ceramic layer from contacting the lithium metal. In particular, a new perovskite Li^+ solid electrolyte, $Li_{0.38}Sr_{0.44}Ta_{0.7}Hf_{0.3}O_{2.95}F_{0.05}$, F-doped to raise its conductivity to $4.8x10^{-4}$ S cm^{-1} at 25 °C, with a thin Li^+-conducting polymer on its surface to prevent reduction of Ta^{5+}, is wet by metallic lithium. Used as a solid electrolyte, excellent cycling performance of an all-solid-state Li//$LiFePO_4$ cell, Li-S cell with a polymer-gel cathode, and a supercapacitor were demonstrated [66].

As an alternative to the insertion of a polymer between the Li-metal layer and the ceramic, plating of lithium through a bed of Li_3N particles is shown to transform dendrite growth into a 3D lithium network formed by wetting the particle surfaces. During Li deposition, Li dendrites can contact Li_3N particles and form solid/solid heterojunctions. Therefore, a space charge layer forms at the Li_3N/Li heterojunction that creates an electric field that attracts Li^+ from the Li_3N to the metallic lithium, the reason why the Li dendrites are suppressed. The Li_3N- modified Li electrode shows a stable cycling performance at 0.5 and 1.0 mA cm^{-2} for more than 100 cycles [67]. Compared to the surface Li_2CO_3 on garnet, Li_3N is not only a good Li^+ conductor but also offers a good wettability with both the garnet surface and a lithium metal anode. As a result, an all-solid-state Li//$LiFePO_4$ battery with a Li_3N-modified garnet also displays high cycling efficiency and stability over 300 cycles even at a temperature of 40 °C [68].

According to another strategy, composite electrolytes consisting of a polymer in which a small amount of ceramic particles are added have been extensively investigated. One reason for choosing a small concentration of nanofillers is that the agglomeration of nanofillers at high concentration has been a major obstacle for improving Li-ion conductivity. However, the Goodenough group designed a three-dimensional (3D) nanostructured hydrogel-derived $Li_{0.35}La_{0.55}TiO_3$ (LLTO) framework, which was used successfully as a 3D nanofiller for high-performance composite polymer Li-ion electrolyte [69]. Then the Goodenough group used Zr-doped LLTO as a filler to propose a “polymer in ceramic” composite, made of a polymer host containing up to 80 wt.% ceramic particles [70]. In this work, the polymer was polyethylene-oxide and the ceramic a garnet, and it turned out they interact so that the ionic conductivity actually decreased when the concentration of garnet increased at such amounts.

Further research is thus needed to select polymer/ceramic couples that maintain or increase the ionic conductivity with the concentration of ceramic. Instead of ceramic particles, hollow mesoporous organic polymer spheres were used in poly(ethylene oxide) (PEO)-filler composite. The cell with this electrolyte in all-solid-state Li//$LiFePO_4$ and Na//$NaTi_2(PO_4)_3$ cells demonstrated stable discharge capacity of approximate to 130 and 80 mAh g^{-1}, respectively, at 0.5C and 65 °C for 100 cycles [71].

As an alternative to ceramic electrolytes that are either easily reduced by Li metal or penetrated by Li dendrites in a short time due to uncontrolled grain boundaries, the Goodenough group introduced a solid electrolyte $LiZr_2(PO_4)_3$ with rhombohedral structure. It reacts with a metallic lithium anode to form a Li^+-conducting passivation layer (solid-electrolyte interphase) containing Li_3P and Li_8ZrO_6 that is wet by the lithium anode and also wets the $LiZr_2(PO_4)_3$ electrolyte. The corresponding Li//$LiFePO_4$ cell showed good cyclability and a long cycle life [72].

The Goodenough group proposed recently an all-solid-state, high voltage cell of long cycle life [73]. The electrolyte consists of a Li_3ClO based-glass electrolyte in a paper nonwoven matrix contacting a lithium anode and a succinonitrile (SN) plasticizer coating a F-Doped Li-Rich Spinel $Li[Li_xNi_{0.5-y}Mn_{1.5-z}]O_{4-x-\delta}F_x$ with $x=y+z$ ~0.36 and $\delta\approx0.36$ (LNMO). Li/Li-glass in paper/SN+LNMO+C+PVDF cell was charged to 5 V versus lithium with a charge/discharge cycle life of over 23,000 cycles at a rate of 153 $mA\cdot g^{-1}$ of active material. The capacity increases with cycling to even exceed the theoretical value due to an electrostatic storage in an EDLC as in a supercapacitor associated to the increasing alignment of the dipoles in the Li^+-glass ferroelectric electrolyte.

With the electrodes and the electrolyte, the separator is the other basic component of the batteries and the Goodenough group also proposed advanced separators to improve their performance and wettability with respect to the commercial ones. In particular colloidal Al_2O_3 particles well dispersed in the PVDF-HFP polymer matrix were found to improve the mechanical strength of the separator that owns a high electrolyte uptake of 372%, a high ionic conductivity of 1.3×10^{-3} S cm^{-1} at 80 °C and only has a 4.5% thermal shrinkage at 150 °C [74]. A PVDF-HFP/colloidal-TiO_2 separator also demonstrates promising potentials for practical applications in high-temperature environments [75].

C. Li-S and Li-air or Li-O2 batteries

Other chemistries, Li-S and Li-air or Li-O_2 are also the subject of intense research since the theoretical capacity of such batteries is much larger than that of the lithium batteries considered in the previous sections. The experiments so far did not reach these promises, but progress is constant.

1. Li-S batteries

For Li-S, two difficulties have to be overcome. (i) the sulfur is an electrical insulator, and the cathode must always be a nano-composite of sulfur with another conductive powder, usually carbon. For instance, sulfur encapsulated in porous hollow carbon nanotubes@carbon nanofibers with 55 wt.% sulfur maintains a capacity of 700 mAh g^{-1} at 1C after 100 cycles and 430 mAh g^{-1} at 5C after 200 cycles [76] (ii) Some of the intermediate lithium polysulfides formed during cycling are soluble in the liquid electrolytes and must be fixed to avoid a shuttling effect between the electrodes. To be comparable with the commercial Li- ion batteries, the capacity density of the sulfur cathode should be higher than 3.3 mAh cm^{-2} considering the average voltage of 2.1 V for Li/S batteries, which requires the loading of sulfur should be higher than 3.3 mg cm^{-2}. To increase the sulfur content/loading, a facile preparation of low- cost nitrogen- doped micro/mesoporous carbon nanofibers (NCF) was proposed [77]. The free-standing multilayers NCF- S membranes used as a cathode of Li-S battery with 1.5 mg cm^{-2} sulfur loading exhibited stable discharge capacities of 1173, 928, and 737 mAh g^{-1} at C/5, C/2, and 1C rates, respectively. Even at a high current density of 2 C rate, a capacity as high as 400 mAh g^{-1} was still achieved. Although the efficiency is just around 98.5%-99.5%, which indicates that the dissolution of polysulfides is not entirely suppressed, this strategy for increasing the sulfur content/loading provide insights on how to develop a commercially viable sulfur cathode for a Li- S rechargeable battery.

As a new strategy, highly cross-linked thiolene polymer electrolyte coating layers with ester electron-donating groups that bind lithium polysulfides has been proposed [78]. This work proved that ester groups on a polymer backbone form lithium bonds with the lithium polysulfides, which brings a significant capacity increase and enhances charge/discharge cycle stability, provided that the bonding is not too strong to hamper Li^+ diffusion and not too weak to trap the lithium polysulfides.

Exploring other conductive substrate than porous carbon for the S cathode architectures, Goodenough et al. proposed mesoporous titanium nitride with a pore-size in the range of 3-20 nm. The TiN- S composite cathode displays a stability better than Vulcan C- S and TiN- S composite cathodes, with a capacity decay of only 0.07% per cycle over 500 charge/discharge cycles, even though the problem of capacity fade was not solved [79].

Layered tungsten disulfide (WS_2) supported both on the cathode current collector and on a carbon cloth interlayer gives excellent performance in a Li-S cell by providing strong adsorption of the soluble Li_2S_x on the WS_2 with fast access to electrons from the current collector via a blocking carbon cloth interlayer. The cell delivered a capacity of 1500 mAh g^{-1} at 0.5 C with a retention of 72.5% at the 500th cycle, and 750 mAh g^{-1} at 5C rate, with electrodes containing 70 wt.% active materials [80] (see Fig.

6).

2. Li-air batteries

Li-air batteries have attracted a lot of attention because of their high theoretical specific energy density (5200 Wh kg^{-1} based on full utilization of a lithium anode. However, these batteries have challenges. The cathode of a lithium–oxygen cell requires a catalyst that is active for both the oxygen-reduction and oxygen-evolution reactions (ORR and OER). Since the discharge product Li_2O_2 is in solid state, it will accumulate at the catalyst surface and hence block the electrode reactions during the discharge process. Meanwhile, during the charging process, it is also difficult to make good contact between the solid catalyst and Li_2O_2. Therefore, many efforts are devoted to the search of such catalysts. Theoretically, the above problems will be alleviated if a solution-phase catalyst is used to catalyze the formation and decomposition of the solid Li_2O_2. This led Sun et al. to report the organic-electrolyte-dissolved iron phthalocyanine (FePc) as a shuttle of O_2^- species and electrons between the surface of the electronic conductor and the insulator Li_2O_2 product of discharge [81]. The Li_2O_2 is observed to grow and decompose without direct contact with carbon, which greatly enhances the electrochemical performance. These results show that the use of molecular shuttles that are catalytically active enable a practical lithium-air rechargeable battery. In the tests, the discharge and charge capacities were limited to 1000 mA h g^{-1}; the discharge current was 0.5 mA cm^{-2}, the charge current was 0.3 mA cm^{-2}. Without the FePc, the cell failed at the 21st cycle; with the aid of FePc, the discharge curves exhibited a flat plateau at 2.69 V fading only to 2.67 V after 130 cycles. Mg-doped perovskite oxides $LaNi_{1-x}Mg_xO_3$ electrolytes can also be used as bi-functional catalysts for lithium air batteries. The reason is that the partial substitution of nickel with magnesium suppresses formation of Ni^{2+} and ensures high concentration of both OER and ORR reaction energy favorable Ni^{3+} (eg = 1) on the surface of perovskite catalysts [82]. α-MnO_2 nanorods grown on porous graphitic carbon nitride (g-C_3N_4) sheets also exhibit high activity for an air cathode, because the α-MnO_2 nanorods catalyze the OER and the porous g- C_3N_4 sheets catalyze the ORR [83].

Ni_3Fe nanoparticles embedded in porous nitrogen-doped carbon sheets (Ni_3Fe/N-C sheets) show excellent catalytic activity, selectivity, and durability toward both the oxygen-reduction and oxygen-evolution reactions [84].

A porous, carbon-free conducting nanopaper, which has dual functions as catalyst and current-collector, was composed of one-dimensional conductive nanowires bound by a chitin binder, enabling the Li-O_2 air electrode to be more stably operated compared to carbon nanofibers [85].

IV. Other chemistries

A. Na-ion batteries

The advantage of sodium is its low price and the huge availability as it can be found in the sea. The drawback is the much lower energy density and voltage of Na-ion based technologies, which will limit the use of Na-ion batteries to a restricted range of applications including electrical grid storage.

1. The positive electrode

Prussian blue (PB) has attracted a lot of attention as a cathode for sodium-ion batteries. It has a small volume change upon cycling [86-88], and the same holds true for rhombohedral Prussian white [89]. The structural stability can even be enhanced by reducing the PB material to the nanoscale, since nanoparticles can accommodate the change of volume more easily. Na-rich prussian blue analogues (PBAs) prepared with different Na^+ concentration solutions by Goodenough et al. exhibited a high reversible capacity of 134 mAh g^{-1} at 0.5C [87]. PBAs have exhibited superiority on the electrochemical properties and material cost, especially Mn- or Fe-based PBAs (such as $Na_2FeMn(CN)_6$ and $Na_2FeFe(CN)_6$). In order to clarify the deviation between the practical capacity and the theoretical one (~170 mAh g^{-1}) and the fast decay of capacity, the roles of interstitial water within hexacyanometallates was systematically investigated [88]. This work gives evidence that uncontrolled $[Fe(CN)_6]$ vacancies and interstitial H_2O in the crystal structure cause poor structural and electrochemical properties, but if further studies of the synthesis of these materials allow to remove such defects, applications can be envisioned. In particular monodispersed PB nanocubes can be nucleated on a CNT conductive network to form a robust and flexible composite cathode material, PB/CNT. At a sub-zero temperature of −25 °C, a PB/CNT cathode can deliver a discharge capacity of 142 mA h g^{-1}, an output specific energy density of 408 Wh kg^{-1}, a high Coulombic efficiency of >99.4%, to give an 86% capacity retention after 1000 cycles [90]. However, most of the Prussian blue materials are still subject to chemical and electrochemical attack in liquid electrolytes, so that they should be combined with a solid electrolytes such as $Na_3Zr_2Si_2PO_{12}$ electrolyte, in which case, a stable cycling performance of an Na-ion cell could be obtained, with a capacity retention of 89.2% after 200 cycles at 0.5C at room temperature [91].

$Na_3V_2(PO_4)_3$, a typical sodium super ionic conductor (NASICON) compound and its derivatives have already been demonstrated with cycle stabilities of over a few thousand cycles by carbon-coating in the surface of particles. Goodenough's group achieved the multi-electron reaction of manganese ions in NASICON-structured $Na_3MnTi(PO_4)_3$ with electrochemical inactive titanium ions. $Na_3MnTi(PO_4)_3$ exhibits high reactive voltages at about 3.6 and 4.1 V with Mn^{2+}/Mn^{3+} and Mn^{3+}/Mn^{4+} redox couples,

respectively [92]. The NASICON-structured $Na_3MnZr(PO_4)_3$ as a cathode for sodium batteries provides discharge voltage plateaus at 3.5 and 4.0 V, only shifted by 0.1V with respect to $Na_3MnTi(PO_4)_3$, and it exhibits an excellent cycling stability, retaining 91% of the initial capacity after 500 charge/discharge cycles at 0.5 C rate [93]. Lately, $Na_4MnV(PO_4)_3$, from which three sodium ion could be reversibly removed (theoretical capacity of 166 mAh g^{-1}), has received much attention. $Na_4MnV(PO_4)_3$ was first prepared by Goodenough's group and delivered an initial capacity of 101 mAh g^{-1} in the voltage range of 2.5–3.8 V with a good cyclic stability over 1000 cycles at 1C [94]. Other sodium phosphates were also proposed, and tested successfully as cathodes for Na-ion batteries: $NaVOPO_4$ [95] and $NaFe_2PO_4(SO_4)_2$ [96].

2. The negative electrode

As recalled in the previous section, either Prussian-blue based materials or NASICON-type of materials can be used as cathodes for Na-ion batteries. Actually, a major obstacle in realizing sodium- ion batteries is the absence of suitable anode materials. Sb is a good candidate, with the use of a sacrificial Na_2NiO_2 source of Na^+ in the cathode to prevent loss of cathode capacity by formation of a SEI on an Sb anode in the initial charge. However, a large volume change between Sb and Na_3Sb alloy leads to poor electrical contact of Sb particles with the conducting matrix, severe pulverization of the Sb particles, and an excess growth of SEI on the fresh Sb surface. A novel polymer network consisting of cross- linked chitosan was designed as a polymer binder to serve as a robust matrix to accommodate the severe volume change of Sb particles during sodiation/desodiation reactions in the anode for sodium- ion batteries. The charge/discharge processes of the Sb electrodes were performed between 0.01 and 2.0 V with sodium foil as the counter electrode, 1 mol L^{-1} $NaClO_4$ in propylene carbonate as electrolyte and fluoroethylene carbonate as additive. It delivered a specific capacity of 555.4 mAh g^{-1} at 1C after 100 cycles, which corresponds to a capacity retention of 96.5% [97].

To meet the requirements of high energy density, it is necessary to replace the hard-carbon anode of the Na-ion battery by a metallic-sodium anode. In this context, a reversible plating/stripping of a dendrite-free metallic-sodium anode with a reduced anode/ceramic interfacial resistance was created by a thin interfacial interlayer formed in situ or by the introduction of a dry polymer film [98]. The polymer used in this work was CPMEA already used to plate a lithium anode [65]. These all-solid-state batteries were obtained with a high cycling stability and Coulombic efficiency at 65 °C.

3. The electrolyte

As soon as in 1967, Goodenough et al. noted that $Na_{1+x}Zr_2P_{3-x}Si_2O_{12}$ is a Na^+-ion conductor, which would be competitive with liquid electrolytes at room temperature, and appears to be easier to fabricate

into dense ceramics than β”-alumina [99]. Since then, like in the case of the lithium batteries, the ability to plate/strip a sodium anode dendrite- free with a Na^+ solid electrolyte motivates investigations of an all- solid- state sodium battery [100]. However, besides the fact that liquid electrolytes have a very high ionic conductivity, their advantage with respect to solid electrolytes is that the liquid can absorb the change in volume of the cathode during cycling, while maintaining contact. An intermediate between solid and liquid, plastic-crystal electrolytes can penetrate into the cathode to access a large fraction of the cathode particles and they deform reversibly with cathode- particle volume change similar to a liquid electrolyte. The Goodenough group reported an application of a plastic–crystal Na^+- electrolyte interphase consisting of succinonitrile complexed with a sodium salt. The terminal nitrile groups do not attract mobile metal ions too strongly and promote charge separation of different metal salts. Taking carbon- coated $Na_3V_2(PO_4)_3$ as the cathode particles and the plastic–crystal electrolyte, the Li-S cell exhibited a stable cycle performance and an excellent rate capability [101]. Note the plastic crystal electrolyte may also provide a universal platform to minimize cathode interfacial resistances in other solid- state battery systems as well.

As an alternative strategy for a safe rechargeable all-solid-state battery, the Goodenough group proposed a Li^+ or Na^+ glass electrolyte that is wet by a metallic lithium or sodium anode, and has a conductivity of 4×10^{-2} S cm^{-1} at room temperature [102]. The result is a safe, low-cost, lithium or sodium rechargeable battery of high energy density and long cycle life.

Like in the case of Li-batteries, the difficulty met with liquid electrolytes and solid-state electrolytes motivated the search for gel-polymer electrolytes that combine a polymer with liquid electrolytes, hoping to combine the positive effects of the two components: mechanical strength owing to the polymer, and good contact with the lithium anode owing to the liquid. A gel-polymer/glass-fiber electrolyte with poly(vinylidene fluoride-co-hexafluoropropylene) (PVDF-HFP) reinforced by a glass-fiber paper and modified by a polydopamine coating, saturated in liquid electrolyte, was tested in a sodium-ion battery with $Na_2MnFe(CN)_6$ as cathode. The results demonstrate that the composite polymer electrolyte is a very attractive separator for a large-scale battery system where safety and cost are the main concerns [103].

4. The separators

The standard polypropylene (PP) separator modified by coating on it a thin layer of reduced graphene oxide (rGO)/sodium lignosulfonate (SL) composite blocks the polysulfides. The reason is that the abundant negatively charged sulfonic groups in the porous lignin network the negatively charged polysulfide (PS) ions without compromising the transport of positively charged Li^+ ions. As a result,

the Li-S battery with this modified separator exhibits a capacity retention of 74% over 1000 cycles [104].

B. K-ion batteries

It is difficult to envision a K^+ battery with high power, since the potassium ion has a higher mass and larger ionic site of K^+ than that of Li^+ and Na^+ and K^+-ion batteries are still investigated only at the laboratory level. However, a cyano-perovskite $K_xMnFe(CN)_6$ ($0 \leq x \leq 2$) was proposed as a potassium cathode: high-spin Mn-III/Mn-II and low-spin Fe-III/F-II couples have similar energies and exhibit two close plateaus centered at 3.6 V. The cathode delivers a specific capacity of 142 mAh g^{-1} [105]. A safe, rechargeable potassium battery of high energy density and excellent cycling stability over 100 cycles was constructed with a polymer-gel electrolyte based on cross- linked poly(methyl methacrylate) (PMMA) [105], polyaniline cathode and KPF_6 salt [106]. The potassium anode wets the polymer, and the cross- linked architecture provides small pores that stabilize a solid- electrolyte interphase formed at the anode/electrolyte interface. The discharge capacity is 138 mAh g^{-1} at a current density of 10 mA g^{-1} and 95 mAh g^{-1} at a current density of 200 mA g^{-1}. These results invite further explorations of new electrolyte and electrode systems in potassium batteries for grid- scale electrical energy storage.

Conclusion

In this review, we have illustrated through few examples the scientific contribution of Professor Goodenough in the chronological order: first as a solid-state physicist, he worked in different areas, including a family of magnetic semiconductors: the perovskites. These materials have applications in electrochemistry, which guided Goodenough to the physical chemistry of the rechargeable batteries. He was one of the Nobel Prize recipients in 2019 for his pioneering work on Li-ion batteries, and his contribution in electrochemistry extends to all the elements of these batteries, anode, cathode, separator, liquid and solid electrolytes, and different chemistries including Li-S, Li-air, Na-ion, and even less mature chemistries like K^+-ion batteries. We can find no better summary of this path than simply cite John Goodenough himself at the ECS Masters, Pennington 2016, also recalled in the ECS Interface 18(4) (2019) in a sentence that will inspire next generations in science: "*I like to think that part of my heritage is that I contributed to the wedding of physics and chemistry. I did not do it alone, of course. We are moving inevitably, inexorably, to interdiciplinarity between physic and material chemistry*".

References

[1] J. B. Goodenough, *J. Appl. Phys*. **1966**, *37*, 1415.

[2] P. M. Raccah, J. B. Goodenough, *Phys. Rev*. **1967**, *155*, 932.

[3] P. M. Raccah, J. B. Goodenough, *J. Appl. Phys*. **1968**, *39*, 1209.

[4] J. S. Zhou, J. B. Goodenough, A. Asamitsu, *Phys. Rev. Lett*. **1997**, *79*, 3234.

[5] M. G. Smith, A. Manthiram, J. Zhou, J. B. Goodenough, J. T. Markert, *Nature* **1991**, *351*, 549.

[6] A. Manthiram, J. S. Swinnea, H. Steinfink, J. B. Goodenough, *J. Amer. Chem. Soc*. **1987**, *109*, 6667.

[7] J. B. Goodenough, A. Manthiram, *J. Solid State Chem*. **1990**, *88*, 115.

[8] A. Manthiram, S. J. Lee, J. B. Goodenough, *J. Solid State Chem*. **1988**, *73*, 278.

[9] J. B. Goodenough, *Superconductor Sci. Tech*. **1990**, *3*, 26.

[10] J. Zhou, J. B. Goodenough, *Phys. Rev. B* **1990**, *42*, 4276.

[11] O. Cyr-Choinière, R. Daou, F. Laliberte, C. Collignon, S. Badoux, D. LeBoeuf, J. Chang, B. J. Ramshaw, D. A. Bonn, W. N. Hardy, R. Liang, J.-Q. Yan, J.-G. Cheng, J.-S. Zhou, J. B. Goodenough, S. Pyon, T. Takayama, H. Takagi, N. Doiron-Leyraud, L. Taillefer, *Phys. Rev*. *B* **2018**, *97*, 064502.

[12] J. B. Goodenough, J. S. Zhou, *Nature* **1997**, *386*, 229.

[13] J. B. Goodenough, *Phys. Rev.* **1955**, *100*, 564.

[14] J. B. Goodenough, *J. Phys. Chem. Solids* **1958**, *6*, 287.

[15] J. Kanamori, *Prog. Theor. Phys*. **1957**, *17*, 177.

[16] J. Kanamori, *J. Phys. Chem. Solids* **1959**, *10*, 87.

[17] J. B. Goodenough, *Magnetism and the Chemical Bond*, Interscience-Wiley, New York, 1963.

[18] J. B. Goodenough, J.-S. Zhou, *Structure and Bonding* **2001**, *98*, 17.

[19] J.-S. Zhou, J. A. Alonso, A. Muoñz, M. T. Fernández-Díaz, J. B. Goodenough, *Phys. Rev. Lett*. **2011**, *106*, 057201.

[20] J.-S. Zhou, J. B. Goodenough, *Phys. Rev. Lett*. **2002**, *89*, 087201.

[21] J.-S. Zhou, J. B. Goodenough, *Phys. Rev. Lett.* **2006**, *96*, 247202.

[22] J. Q. Yan, L. S. Zhou, J. B. Goodenough, *Phys. Rev*. *B* **2004**, *70*, 014402.

[23] J. B. Goodenough and J. M. Longo, in *Crystallographic and Magnetic Properties of Perovskite and Perovskite-Related Compounds*, vol. 4A, (Ed.: K.-H. Hellwege), Springer-Verlag, Berlin, 1970, p. 126.

[24] H. C. Nguyen, J. B. Goodenough, *Phys. Rev. B* **1995**, *52*, 324.

[25] J. B. Goodenough, *National Academy of Engineering*, https://www.nae.edu/105796/John-B-

Goodenough. Accessed Nov. 5, 2019.

[26] J. Suntivich, H. A. Gasteiger, Y. N. Yabuuchi, N. H. Nakanishi, J. B. Goodenough, Y. Shao-Horn, *Nature Chem*. **2011**, *3*, 546.

[27] Z. Mousavi, F. Soofivand, M. Esmaeili-Zare, M. Salavati-Niasari, S. Bagheri, *Sci. Rep.* **2016**, *6*, 20071.

[28] J. B. Goodenough, A. L. Loeb, *Phys. Rev*. **1955**, *98*, 391.

[29] C. M. Julien, A. Mauger, A. Vijh, K. Zaghib, *Lithium Batteries: Science and Technology*, Springer, Cham, 2016.

[30] H. Zhang, C. Li, G. G. Eshetu, S. Laruelle, S. Grugeon, K. Zaghib, C. M. Julien, A. Mauger, D. Guyomard, T. Rojo, N. Gisbert-Trejo, S. Passerini, X. Huang, Z. Zhou, P. Johansson, M. Forsyth, *Angew. Chem. Int. Ed*. **2020**, *132*, 542.

[31] K. Mizushima, P. C. Jones, P. J. Wiseman, J. B. Goodenough, *Mater. Res. Bull*. **1980**, *15*, 783.

[32] J. B. Goodenough, K. Mizushima, *US Patent* 4,302,518 (Nov. 24, 1981).

[33] M.M. Thackeray, J. Coetzer, *Mater. Res. Bull*. **1981**, *16*, 591.

[34] M.M. Thackeray, W.I.F. David, J.B. Goodenough, *Mater. Res. Bull*. **1982**, *17*, 785.

[35] M. M. Thackeray, W. I. F. David, P. G. Bruce, J. B. Goodenough, *Mat. Res. Bull*. **1983**, *18*, 461.

[36] L. Wang, X. Zhao, Y. Lu, M. Xu, D. Zhang, F. Ruoff, K. Stevenson, J. Kate, J. B. Goodenough, *J. Electrochem. Soc*. **2011**, *158*, A1379.

[37] J. Song, D. W. Shin, Y. H. Lu, C. D. Amos, A. Manthiram, J. B. Goodenough, *Chem. Mater*. **2012**, *24*, 3101.

[38] D. Liu, W. Zhu, J. Trottier, C. Cagnon, F. Barray, A. Guerfi, A. Mauger, H. Groult, C. M. Julien, J. B. Goodenough, K. Zaghib, *RSC Adv*. **2014**, *4*, 154.

[39] D. Liu, J. Hamel-Paquet, J. Trottier, F. Barray, V. Gariepy, P. Hovington, A. Guerfi, A. Mauger, C. M. Julien, J. B. Goodenough, K. Zaghib, *J. Power Sources* **2012**, *217*, 400.

[40] A. K. Padhi, K. S. Nanjundaswamy, *J. Electrochem. Soc*. **1997**, *144*, 1188.

[41] A. K. Padhi, K. S. Nanjundaswamy, C. Masquelier, S. Okada, J. B. Goodenough, *J. Electrochem. Soc*. **1997**, *144*, 1609.

[42] J. B. Goodenough, *J. Phys. Chem. Solids* **1964**, *25*, 151.

[43] K.-S. Park, S. B. Schougaard, J. B. Goodenough, *Adv. Mater*. **1976**, *19*, 848.

[44] Y.-H. Huang, J. B. Goodenough, *Chem. Mater.* **2008**, *20*, 7237.

[45] Y. H. Huang, K. S. Park, J. B. Goodenough, *J. Electrochem. Soc*. **2006**, *153*, A2282.

[46] K. Zaghib, A. Mauger, H. Groult, J. Goodenough, C. M. Julien, *Materials* **2013**, *6*, 1028.

[47] A. A. Ait-Salah, A. Mauger, K. Zaghib, J. B. Goodenough, N. Ravet, M. Gauthier, F. Gendron, C. M. Julien, *J. Electrochem. Soc*. **2006**, *153*, A1692.

[48] N. Ravet, K. Zaghib, M. Gauthier, J. Goodenough, A. Mauger, F. Gendron, C. M. Julien, *Chem. Mater*. **2007**, *19*, 2595.

[49] K. Zaghib, A. Mauger, J. B. Goodenough, C. M. Julien, F. Gendron, *Chem. Mater*. **2007**, *19*, 3740.

[50] K. Zaghib, N. Ravet, M. Gauthier, F. Gendron, A. Mauger, J. B. Goodenough, C. M. Julien, *J. Power Sources* **2006**, *163*, 560.

[51] K. Zaghib, A. Guerfi, P. Hovington, M. Trudeau, A. Mauger, J. B. Goodenough, C. M. Julien, *J. Power Sources* **2013**, *232*, 357.

[52] A. Mauger, C. M. Julien, M. Armand, J. B. Goodenough, K. Zaghib, *Current Opinion in Electrochem*. **2017**, *6*, 63.

[53] B. C. Yu, K. Park, J.-H. Yang, J. B. Goodenough, *ACS Energy Lett*. **2016**, *1*, 633-637.

[54] X. Shen, Y. Li, T. Qian, J. Liu, J. Zhou, C. Yan, J. B. Goodenough, *Nature Commun*. **2019**, *10*, 900.

[55] J. Liu, Z. Bao, Y. Cui, E. J. Dufek, J. B. Goodenough, P. Khalifah, Q. Li, B. Y. Liaw, A.Manthiram, Y. S. Meng, V. R. Subramanian, M. F. Toney, V. V. Wiswanathan, M. S. Whittingham, J. Xiao, W. Xu, J. Yang, X.-Q. Yang, J.-G. Zhang, *Nature Energy* **2019**, *4*, 180.

[56] Y. Li, B. Xu, H. Xu, H. Duan, X. Lu, S. Xin, Z. Zhou, L. Xue, G. Fu, A. Manthiram, J. B. Goodenough, *Angew. Chem. Int. Ed*. **2017**, *56*, 753.

[57] W. Zhou, Z. Wang, Y. Pu, Y. Li, S. Xin, X. Li, J. Chen, J. B. Goodenough, *Adv. Mater*. **2019**, *31*, 1805574.

[58] J. B. Goodenough, *Solid State Ionics* **1997**, *94*, 17.

[59] Y. T. Li, J.-T. Han, C.-A. Wang, S. C. Vogel, H. Xie, M. Xu, J. B. Goodenough, *J. Power Sources* **2012**, *209*, 278.

[60] Y. T. Li, C.-A. Wang, H. Xie, J. Cheng, J. B. Goodenough, *Electrochem. Commun*. **2011**, *13*, 1289.

[61] K. Park, B. C. Yu, J.-W. Jung, Y. Li, W. D. Zhou, H. C. Gao, S. Son, J. B. Goodenough, *Chem. Mater*. **2016**, *28*, 8051.

[62] Y. T. Li, J. T. Han, C.-A. Wang, H. Xie, J. B. Goodenough, *J. Mater. Chem*. **2012**, 22, 15357.

[63] Y. T. Li, X. Chen, A. Dolocan, Z. Cui, S. Xin, L. Xue, H. Xu, K. Park, J. B. Goodenough, *J. Amer. Chem. Soc*. **2018**, 140, 6448.

[64] W. Zhou, Y. Zhu, N. Grundish, S. Xin, S. Wang, Y. You, N. Wu, J. Gao, Z. Cui, Y. Li, J. B. Goodenough, *Nano Energy* **2018**, *45*, 413.

[65] W. Zhou, S. Wang, Y. Li, S. Xin, A. Manthiram, J. B. Goodenough, *J. Am. Chem. Soc.* **2016**, *138*, 9385.

[66] Y. Li, H. Xu, P. Chien, N. Wu, S. Xin, L. Xue, K. Park, Y. Hu, J. B. Goodenough, *Angew. Chem. Int. Ed*. **2018**, *57*, 8587.

[67] K. Park, J. B. Goodenough, *Adv. Energy Mater*. **2017**, *7*, 1700732.

[68] H. Xu, Y. Li, A. Zhou, N. Wu, S. Xin, Z. Li, J. B. Goodenough, *Nano Lett*. **2018**, *18*, 7414.

[69] J. Bae, Y. T. Li, J. Zhang, X. Zhou, F. Zhao, Y. Shi, J. B. Goodenough, G. Yu, *Angew. Chem. Int. Ed*. **2018**, *57*, 2096.

[70] L. Chen, Y. Li, S.-P. Li, L.-Z. Fan, C.-W. Nan, J. B. Goodenough, *Nano Energy* **2018**, *46*, 176.

[71] W. Zhou, H. Gao, J. B. Goodenough, *Adv. Energy Mater*. **2016**, *6*, 1501802.

[72] Y. Li, W. Zhou, X. Chen, X. Lu, Z. Cui, S. Xin, L. Xue, Q. Jia, J. B. Goodenough, *Proc. of The Nat. Acad. Sci. USA* **2016**, *113*, 13313.

[73] M. H. Braga, C. M. Subramaniyam, A. J. Murchison, J. B. Goodenough, *J. Am. Chem. Soc*. **2018**, *140*, 6343.

[74] S. Ali, C. Tan, M. Waqas, W. Lv, Z. Wei, S. Wu, B. Boateng, J. Liu, J. Ahmed, J. Xiong, J. B. Goodenough, W. He, *Adv. Mater. Interfaces* **2018**, *5*, 1701147.

[75] M. Waqas, C. Tan, W. Lv, S. Ali, B. Boateng, W. Chen, Z. Wei, C. Feng, J. Ahmed, J. B. Goodenough, W. He, *ChemElectroChem* **2018**, *5*, 2722.

[76] Y. Chen, X. Li, K.-S. Park, J. Hong, J. Song, L. Zhou, Y.-W. Mai, H. Huang, J. B. Goodenough, *J. Mater. Chem*. **2014**, *2*, 10126.

[77] W. Zhou, B. Guo, J. B. Goodenough, *Adv. Energy Mater*. **2016**, *6*, 1502059.

[78] K. Park, J. H. Cho, J.-H. Jang, B.-C. Yu, A. T. De La Hoz, K. M. Miller, C. J. Ellison, J. B. Goodenough, *Energy Environ. Sci*. **2015**, *8*, 2389.

[79] Z. Cui, C. Zu, W. Zhou, A. Manthiram, J. B. Goodenough, *Adv. Mater*. **2016**, **28**, 6926.

[80] J. Park, B.-C. Yu, J. S. Park, J. W. Choi, C. Kim, Y.-E. Sung, J. B. Goodenough, *Adv. Energy Mater*. **2017**, *7*, 1602567.

[81] D. Sun, Y. Shen, W. Zhang, L. Yu, Z. Yi, W. Yin, D. Wang, Y. Huang, J. Wang, D. Wang, J. B. Goodenough, *J. Am. Chem. Soc.* **2014**, *136*, 25, 8941.

[82] Z. Du, P. Yang, L. Wang, Y. Lu, J. B. Goodenough, J. Zhang, D. Zhang, *J. Power Sources* **2014**, *265*, 91.

[83] Y. Hang, C. Zhang, X. Luo, Y. Xie, S. Xi, Y. Li, D. Zhang, J. B. Goodenough, *J. Power Sources* **2018**, *392*, 15.

[84] G. Fu, Z. Cui, Y. Chen, Y. Li, Y. Tang, J. B. Goodenough, *Adv. Energy Mater.* **2017**, *7*, 1601172.

[85] J.-W. Jung, H.-G. Im, D. Lee, S. Yu, J.-H. Fang, K. R. Yoon, Y. H. Kim, J. B. Goodenough, J. Jin, I.-D. Kim, B. S. Bae, *ACS Energy Lett*. **2017**, *2*, 673.

[86] Y. Lu, L. Wang, J. G. Cheng, J. B. Goodenough, *Chem. Commun*. **2012**, *48*, 6544.

[87] L. Wang, Y. Lu, J. Liu, M. Xu, J. Cheng, D. Zhang, J. B. Goodenough, *Angew. Chem. Int. Ed*. **2013**, *52*, 1964.

[88] J. Song, L. Wang, Y. Lu, J. Liu, B. Guo, P. Xiao, J.-J. Lee, X.-Q. Yang, G. Henkelman, J. B. Goodenough, *J. Am. Chem. Soc*. **2015**, *137*, 2658.

[89] L. Wang, J. Song, R. M. Qiao, L. A. Wray, M. A. Hossain, Y.-D. Chuang, W. yang, Y. Lu, D. Evans, J.-J. lee, S. Vail, X. Zhao, M. Nishijima, S. Kakimoto, J. B. Goodenough, *J. Amer. Chem. Soc*. **2015**, *137*, 2548.

[90] Y. You, H.-R. Yao, S. Xin, Y.-X. Yin, T.-T. Zuo, C.-P. Yang, Y.-G. Guo, Y. Cui, L.-J. Wan, J. B. Goodenough, *Adv. Mater*. **2016**, *28*, 7243.

[91] H. Gao, S. Xin, L. Xue, J. B. Goodenough, *Chem*. **2018**, *4*, 833.

[92] H. Gao, Y. Li, K. Park, J.B. Goodenough, *Chem. Mater*. **2016**, *28*, 6553.

[93] H. Gao, I. D. Seymour, S. Xin, L. Xue, G. Henkelman, J. B. Goodenough, *J. Amer. Chem. Soc*. **2018**, *140*, 18192.

[94] W. Zhou, L. Xue, X. Lu, H. Gao, Y. Li, S. Xin, G. Fu, Z. Cui, Y. Zhu, J.B. Goodenough, *Nano Lett*. **2016**, *16*, 7836.

[95] J. Song, M. Xu, L. Wang, J. B. Goodenough, *Chem. Commun*. **2013**, *49*, 5280.

[96] K. Shiva, P. Singh, W. Zhou, J. B. Goodenough, *Energy Environ. Sci*. **2016**, *9*, 3103.

[97] H. Gao, W. Zhou, J.-H. Jang, J. B. Goodenough, *Adv. Energy Mater*. **2016**, *6*, 1502130.

[98] W. Zhou, Y. Li, S. Xin, J. B. Goodenough, *ACS Cent. Sci.* **2017**, *3*, 52.

[99] J. B. Goodenough, H. Y-P. Hong, J. A. Kafalas, *Mat. Res. Bull*. **1976**, *2*, 203.

[100] J. B. Goodenough, *Energy Environ. Sci*. **2014**, *7*, 14.

[101] H. Gao, L. Xue, S. Xin, K. Park, J. B. Goodenough, *Angew. Chem. Int. Ed*. **2017**, *56*, 5541.

[102] M. H. Braga, N. S. Grundish, A. J. Murchison, J. B. Goodenough, *Energy Environ. Sci.* **2017**, *10*, 331.

[103] H. Gao, B. Guo, J. Song, K. Park, J. B. Goodenough, *Adv. Energy Mater*. **2015**, *5*, 1402235.

[104] T. Lei, W. Chen, W. Lv, J. Huang, J. Zhu, J. Chu, C. Yan, C. Wu, Y. Yan, W. He, J. Xiong, Y. Li, C. Yan, J. B. Goodenough, X. Duan, *Joule* **2018**, *2*, 2091.

[105] L. G. Xue, Y. T. Li, H. C. Gao, W. D. Zhou, X. J. Lu, W. Kaveevivitchai, A. Manthiram, J. B.

Goodenough, *J. Amer. Chem. Soc*. **2017**, *139*, 2164.

[106] H. C. Gao, W. D. Zhou, K. Park, J. B. Goodenough, *Adv. Energy Mater.* **2016**, *6*, 1600467.

[107] H. Gao, L. Xue, S. Xin, J. B. Goodenough, *Angew. Chem. Int. Ed*. **2018**, *57*, 5449.

Figure captions

Figure 1. Crystallographic structure of AMO_3 perovskite in the cubic and orthorhombic phase. *M* is a transition metal. Open circles are oxygen sites.

Figure 2. Temperature dependence of magnetic moment *M* at Cr^{3+} in $LaCrO_3$ under three different pressures; the inset shows the blowup plot of *M*(*T*) under P = 5.5 GPa. Solid lines inside the figure are curve fittings to the Brillouin function. Reproduced with permission from [18]. Copyright 2001 Springer.

Figure 3. Cycling performance and Coulombic efficiency of $LiMn_{1.45}Cr_{0.1}Ni_{0.45}O_4$. Reproduced with permission from [38]. Copyright 2014 Royal Society of Chemistry.

Figure 4. Small magnetic polaron in $LiFePO_4$. The hopping process is illustrated in (a). The $t_g\downarrow$ "hole" on the Fe^{3+} site 1 is shifted to a neighboring iron site 2 by transfer of one $t_g\downarrow$ electron from site 2 to site 1. The indirect exchange interaction is responsible for the spin-polarization of the iron ions inside the electronic $t_g\downarrow$ "hole" wavefunction (in the direction opposite to that of the t_g electron), as it is illustrated in (b). As the charge in excess hops from site to site, it brings with it not only a local lattice deformation cloud associated with the Coulomb potential but also its spin-polarization cloud. Reproduced with permission from [48]. Copyright 2007 The American Chemical Society.

Figure 5. Schematic of Li-metal batteries with garnet LLZT and LLZT-C. In LLZT, the surface Li_2CO_3 layer and H^+ exchanged H-LLZT phase block the Li^+ transport across the garnet/electrode interface; the lithium dendrites grow fast owing to the uneven distribution of current density. In carbon-treated LLZT (LLZT-C), the interfacial resistances of Li/garnet, garnet/electrolyte, and garnet/cathode become very small due to the removal of the Li^+ blocking layer at the surface of the garnet grain. Reproduced with permission from [62]. Copyright 2012 Royal Society of Chemistry.

Figure 6. Tungsten Disulfide Catalysts Supported on a Carbon Cloth Interlayer for High Performance Li–S Battery. (a) Cycle retention of S, S/WS_2, S–CCI, and WS_2/S–WS_2/CCI at 0.05 C rate until 100 cycles and (b) those capacity versus voltage profiles. Discharge profiles of (c) the upper plateau and slope regions and (d) lower plateau region. Internal resistance change of (e) upper plateau and slope

regions and (f) lower plateau region during discharge derived by GITT. Reproduced with permission from [79] Copyright 2016 Wiley.

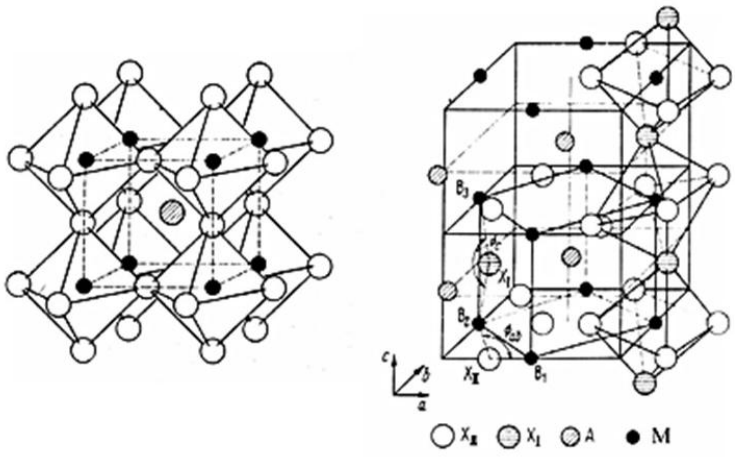

Figure 1.

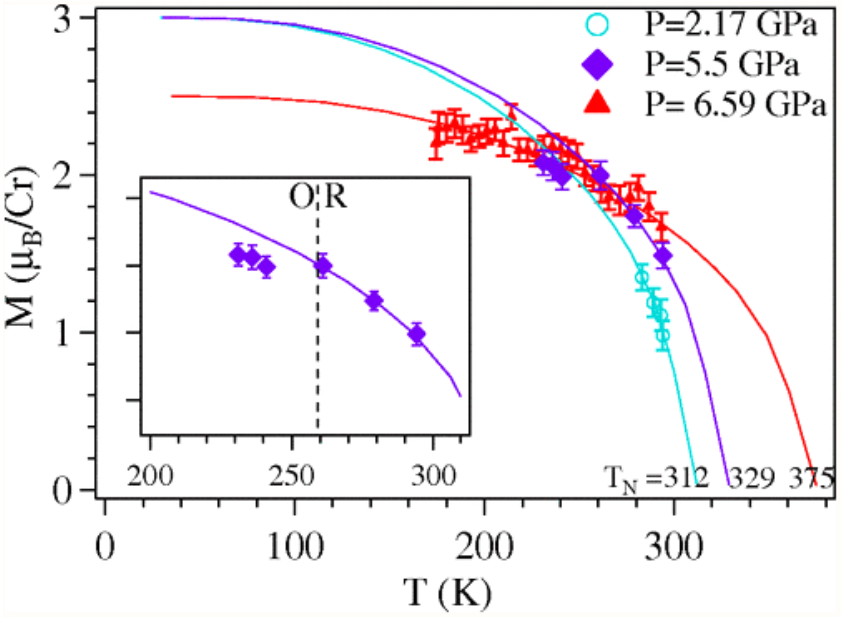

Figure 2.

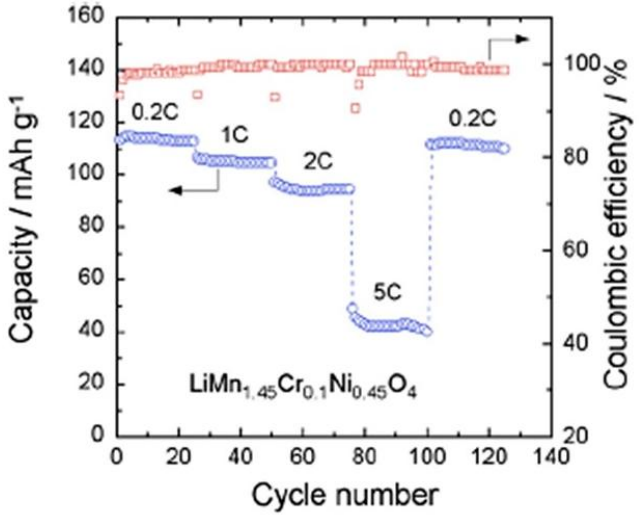

Figure 3.

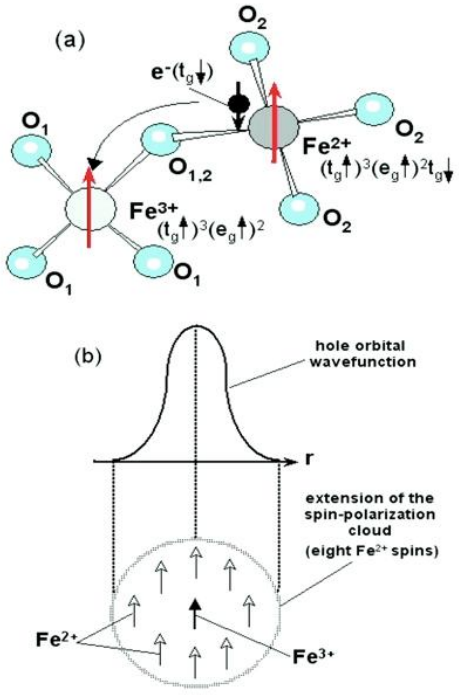

Figure 4.

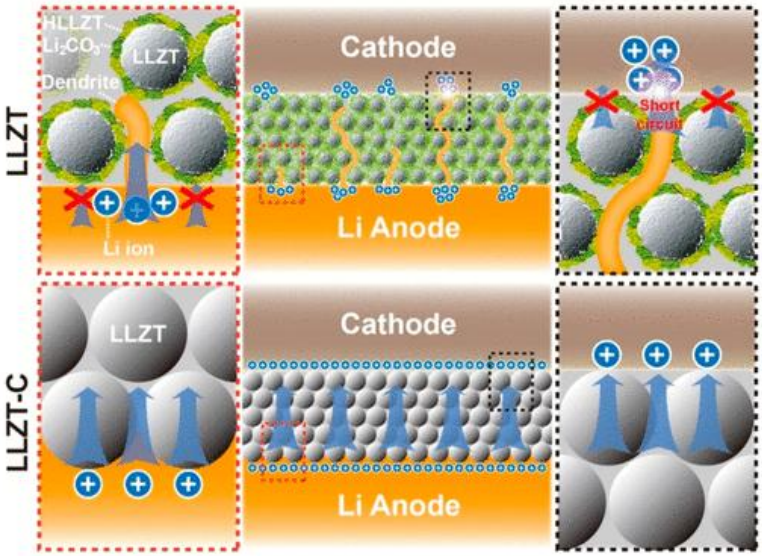

Figure 5.

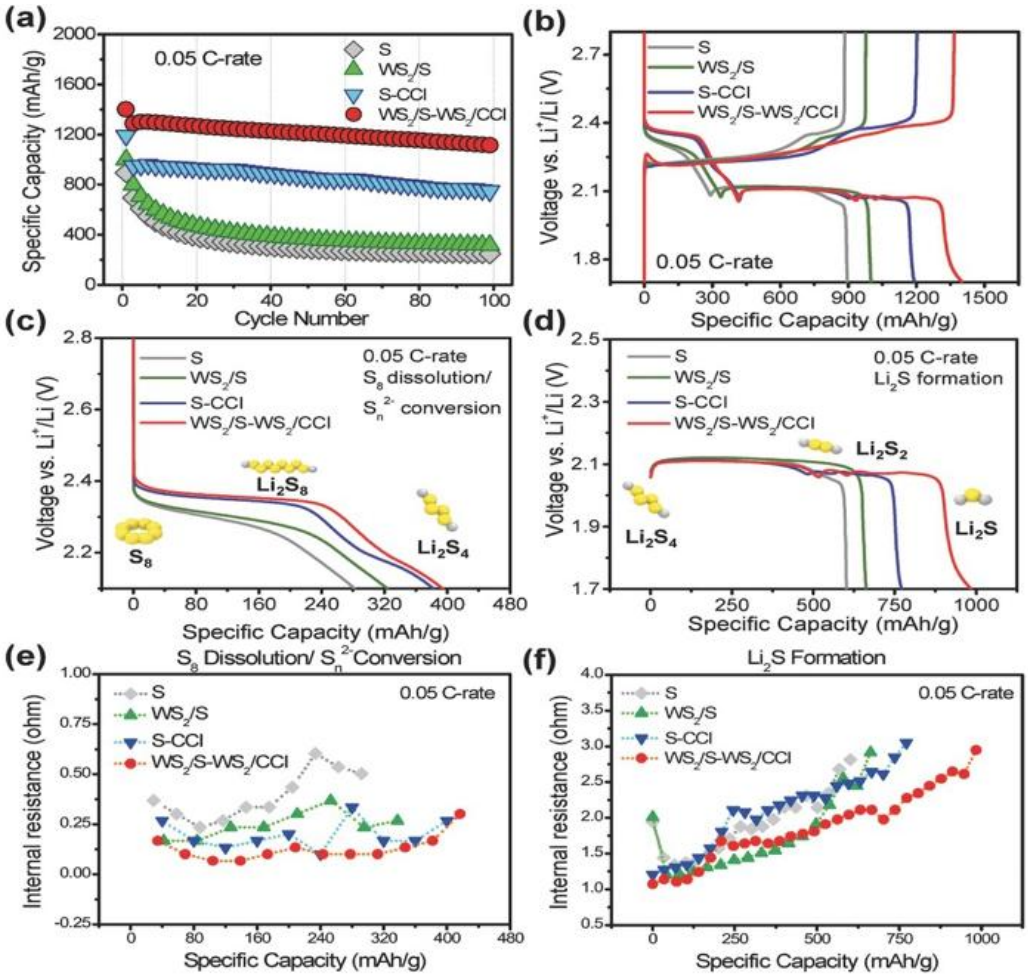

Figure 6.